# Local refractive index sensitivity of gold nanodisks

**Verena Häfele,[*] Andreas Trügler, Ulrich Hohenester, Andreas Hohenau, Alfred Leitner, and Joachim R. Krenn**

*Institute of Physics, University of Graz, Universitätsplatz 5, 8010 Graz, Austria*
[*]*verena.haefele@uni-graz.at*

**Abstract:** We experimentally investigate the local refractive index sensitivity of plasmonic gold nanodisks by applying small polymer dots to selected disk sites by means of two-step lithography. Measured sensitivity profiles obtained from tracking the polymer-induced spectral shift of the plasmon modes are in excellent agreement with numerical simulation of both spectral sensitivity and the electric near field of the nanodisks. Based on the nanodisk sensitivity profile we tailor a sensitive and spatially uniform plasmonic sensor by capping the disk with a dielectric layer, thus restricting analyte access to the disk rim.



**OCIS codes:** (220.4241) Nanostructure fabrication; (240.6680) Surface plasmons; (280.4788) Optical sensing and sensors; (310.6628) Subwavelength structures, nanostructures.

## References and links

1. L. Novotny and B. Hecht, *Principles of Nano-Optics* (Cambridge University, 2012).
2. E. Prodan, C. Radloff, N. J. Halas, and P. Nordlander, "A Hybridization Model for the Plasmon Response of Complex Nanostructures," Science **302**(5644), 419–422 (2003).
3. K. L. Kelly, E. Coronado, L. L. Zhao, and G. C. Schatz, "The optical properties of metal nanoparticles: the influence of size, shape, and dielectric environment," J. Phys. Chem. B **107**(3), 668–677 (2003).
4. K. M. Mayer and J. H. Hafner, "Localized surface plasmon resonance sensors," Chem. Rev. **111**(6), 3828–3857 (2011).
5. E. Petryayeva and U. J. Krull, "Localized surface plasmon resonance: Nanostructures, bioassays and biosensing - A review," Anal. Chim. Acta **706**(1), 8–24 (2011).
6. S. Roh, T. Chung, and B. Lee, "Overview of the Characteristics of Micro- and Nano-Structured Surface Plasmon Resonance Sensors," Sensors (Basel) **11**(12), 1565–1588 (2011).
7. A. G. Brolo, "Plasmonics for future biosensors," Nat. Photonics **6**(11), 709–713 (2012).
8. A. B. Dahlin, N. J. Wittenberg, F. Hook, and S.-H. Oh, "Promises and challenges of nanoplasmonic devices for refractometric biosensing," Proc. Soc. Photo-Opt. Ins. **2**(2), 83–101 (2013).
9. M. Piliarik, P. Kvasnička, N. Galler, J. R. Krenn, and J. Homola, "Local refractive index sensitivity of plasmonic nanoparticles," Opt. Express **19**(10), 9213–9220 (2011).
10. I. Ament, J. Prasad, A. Henkel, S. Schmachtel, and C. Sönnichsen, "Single unlabeled protein detection on individual plasmonic nanoparticles," Nano Lett. **12**(2), 1092–1095 (2012).
11. E. C. Le Ru, J. Grand, I. Sow, W. R. C. Somerville, P. G. Etchegoin, M. Treguer-Delapierre, G. Charron, N. Félidj, G. Lévi, and J. Aubard, "A Scheme for Detecting Every Single Target Molecule with Surface-Enhanced Raman Spectroscopy," Nano Lett. **11**(11), 5013–5019 (2011).
12. M. Schnell, A. García-Etxarri, A. J. Huber, K. Crozier, J. Aizpurua, and R. Hillenbrand, "Controlling the near-field oscillations of loaded plasmonic nanoantennas," Nat. Photonics **3**(5), 287–291 (2009).
13. T. Geldhauser, A. Kolloch, N. Murazawa, K. Ueno, J. Boneberg, P. Leiderer, E. Scheer, and H. Misawa, "Quantitative measurement of the near-field enhancement of nanostructures by two-photon polymerization," Langmuir **28**(24), 9041–9046 (2012).
14. D. M. Koller, U. Hohenester, A. Hohenau, H. Ditlbacher, F. Reil, N. Galler, F. R. Aussenegg, A. Leitner, A. Trügler, and J. R. Krenn, "Superresolution Moiré mapping of particle plasmon modes," Phys. Rev. Lett. **104**(14), 143901 (2004).
15. F. Ph. Schmidt, H. Ditlbacher, U. Hohenester, A. Hohenau, F. Hofer, and J. R. Krenn, "Dark plasmonic breathing modes in silver nanodisks," Nano Lett. **12**(11), 5780–5783 (2012).
16. T. J. Davis, D. E. Gómez, and K. C. Vernon, "Interaction of molecules with localized surface plasmons in metallic nanoparticles," Phys. Rev. B **81**(4), 045432 (2010).
17. V. Claudio, A. B. Dahlin, and T. J. Antosiewicz, "Single-particle Plasmon sensing of discrete molecular events: binding position versus signal variations for different sensor geometries," PhysChemComm **118**(13), 6980–6988 (2014).

#228502 - $15.00 USD Received 24 Nov 2014; revised 26 Feb 2015; accepted 3 Mar 2015; published 14 Apr 2015

18. T. Kalkbrenner, U. Håkanson, and V. Sandoghdar, "Tomographic plasmon spectroscopy of a single gold nanoparticle," Nano Lett. **4**(12), 2309–2314 (2004).
19. A. B. Dahlin, J. O. Tegenfeldt, and F. Höök, "Improving the instrumental resolution of sensors based on Localized Surface Plasmon Resonance," Anal. Chem. **78**(13), 4416–4423 (2006).
20. U. Hohenester and A. Trügler, "A Matlab toolbox for the simulation of plasmonic nanoparticles," Comput. Phys. Commun. **183**(2), 370–381 (2012).
21. F. J. Garcia de Abajo and A. Howie, "Retarded field calculation of electron energy loss in inhomogeneous dielectrics," Phys. Rev. B **65**(11), 115418 (2002).
22. P. B. Johnson and R. W. Christy, "Optical constants of the noble metals," Phys. Rev. B **6**(12), 4370–4379 (1972).
23. T. J. Antosiewicz, S. P. Apell, V. Claudio, and M. Käll, "A simple model for the resonance shift of localized plasmons due to dielectric particle adhesion," Opt. Express **20**(1), 524–533 (2012).
24. W. A. Murray, J. R. Suckling, and W. L. Barnes, "Overlayers on silver nanotriangles: field confinement and spectral position of localized surface plasmon resonances," Nano Lett. **6**(8), 1772–1777 (2006).

## 1. Introduction

Metal nanoparticles (NP) feature plasmonic excitations, so-called localized surface plasmon resonances (LSPR), which are characterized by strong light absorption and scattering and a strong optical near field [1]. By shaping the NP geometry, the plasmonic modes can be tailored, resulting in specific resonance frequencies and electromagnetic near field profiles. For example, morphing a metal nanosphere into an ellipsoidal particle causes the resonances along the long axis to redshift and leads to the appearance of strongly enhanced fields at the tips of the elongated NP. Likewise, enhanced fields generated by plasmon hybridization can be found in gaps between two NPs [2].

One of the most promising applications for LSPR is refractometric sensing, as changes in the refractive index of the surrounding medium affect the resonance frequency of NPs. This feature makes LSPR particularly useful for label-free bio-sensor applications [3–8]. Importantly, the NP near field is usually strongly inhomogeneous. As a NP's optical response to analyte access depends on the spatial overlap of the particle near field and the analyte distribution [9], this leads to an inhomogeneous, i.e., position dependent sensitivity. This inhomogeneous sensitivity affects the total signal upon molecular binding and it can impede quantitative measurement at low concentrations due to binding at sites of strongly different sensitivity [10]. It has been suggested to restrict the binding of analyte molecules to selected areas of the particle surface that exhibit well-defined sensitivity values. Le Ru et al. [11], for example, chemically blocked the access of analyte molecules to the surface of gold bipyramids, except at the particle tips where the field is strongest. To pursue this approach of controlled analyte access, it is necessary to study in detail the NP field and sensitivity distribution. Plasmonic modes of tailored nanoparticles have been studied with various methods, as with scanning near-field optical microscopy [12], plasmon-field dependent polymerization [13], the position-dependent spontaneous lifetime of fluorophores [14] or electron energy loss spectroscopy combined with electron microscopy [15].

The sensitivity of LSPR was probed by means of local modifications in the refractive index of the surrounding medium. Davis et al. [16] and Claudio et al. [17] followed this approach theoretically by looking at the spectral response of NPs upon the adhesion of a small dielectric sphere to different areas on the NP surface. A position-dependent shift in the NP resonance frequency was found, corresponding to the inhomogeneous field distribution. Kalkbrenner et al. [18] experimentally investigated how the spectrum of a gold NP is influenced upon the approach of a glass tip. Piliarik et al. [9] characterized the local refractive index sensitivity of gold nanoparticles by applying polymer stripes to well defined particle areas, showing that the sensitivity is correlated with the local electric field strengths of the NPs.

In this work, we experimentally analyze the local refractive index sensitivity of gold nanodisks by attaching small polymer dots at defined position at their surface. Such dots can be considered as a model system for the adhesion of large analyte molecules. The directed attachment of the dots to the NPs are, to the best of our knowledge, the first experimental corroboration of local sensitivity distribution calculations on a three-dimensional system as performed by Davis et al. [16]. With our method the sensitivity distribution of arbitrarily

#228502 - $15.00 USD Received 24 Nov 2014; revised 26 Feb 2015; accepted 3 Mar 2015; published 14 Apr 2015

shaped NPs can be directly measured, allowing for a better understanding of the sensing process and for potentially improving the sensitivity of plasmonic NP probes.

## 2. Plasmonic nanodisks with polymer dots

Arrays of gold nanodisks were fabricated by electron beam lithography using the positive resist poly(methyl methacrylate) (PMMA) on an indium-tin-oxide covered glass substrate. After electron exposure and chemical development, gold was evaporated onto the resulting PMMA mask, followed by lift-off. Nanoparticle dimensions, measured in a scanning electron microscope (SEM), were 150 ± 3 nm in diameter, with a height of 30 ± 1 nm. To fabricate the polymer dots the negative tone resist SU-8-3010 (MicroChem Corp.), diluted with SU-8 thinner (MicroChem Corp.) at a ratio of 1:15, was spin coated on the nanoparticle arrays. The spin-coated polymer layer followed the underlying structure to some extent, having a height of 70 nm on the substrate and 60 nm on the gold disks, as measured from atomic force microscopy. Electron beam exposure yielded cylindrical polymer dots with 50 ± 3 nm in diameter at specific positions of the NP surface. The alignment of the polymer dots with the disk arrays was achieved by using a set of alignment markers. Large alignment markers were used for coarse positioning of the dot structure with respect to the disks, 0.3 µm sized markers helped to align the polymer dots to the nanodisks with an accuracy of ± 5 nm.

The NPs were illuminated by a 50 W tungsten white light source under dark field illumination in a Nikon TE2000-S microscope. The scattered light was collected with a 40 x, numerical aperture = 0.75 microscope objective (Nikon, Plan Fluor) and imaged onto the 20 µm wide slit of a photospectrometer (monochromator Andor, Shamrock SR-303i and camera Andor, iXon DV885LC). The LSPR spectra were evaluated by calculating the centroid (center of mass) of the LSPR peak [19]. The spectral resolution of the measurement setup and the used centroid method for data evaluation yielded a peak position precision of <0.1 nm.

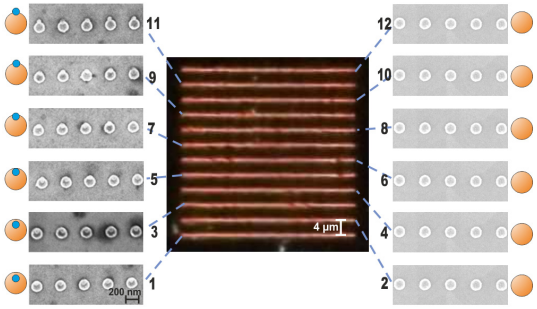


Fig. 1. Overview of the row-based sample design. The central panel depicts an optical microscope dark field image of the two-dimensional arrangement of particle rows. The left and right panels show SEM images of rows of dotted and bare gold nanodisks, respectively, and sketches of the nanodisks (golden) and polymer dots (blue).

The effect on the NP resonance frequency caused by the attached polymer dot could in principle be determined by comparing a modified NP (in the following we will refer to NPs modified with polymer dots as "dotted" NPs) with an adjacent, unmodified ("bare") particle as a reference. However, due to small fabrication-related geometric differences between individual NPs, their plasmonic resonance wavelengths fluctuate by a few nm. As the expected shift of the NP resonance frequency due to the presence of the polymer dots lies in the same range, it is not possible to base our measurements on single NPs. Alternatively, we employ a row-based sample design, as shown in Fig. 1. Gold nanodisks were arranged in a two-dimensional pattern consisting of 12 parallel rows, each row consisting of 147 particles with a mutual distance of 320 nm. By averaging over the spectra of all particles in one row the influence of the particle geometry deviations on the spectral signature was practically eliminated. The distance between individual rows was chosen as 4 µm to obtain closely spaced rows that still can be probed separately by microscopic imaging.

#228502 - $15.00 USD Received 24 Nov 2014; revised 26 Feb 2015; accepted 3 Mar 2015; published 14 Apr 2015

The nanodisks in every other row were modified in the second lithography step by adding the polymer dots, while the NPs in the rows in between remained bare and served as a reference. The effect of the polymer dots on the plasmonic nanodisk resonance was deduced by comparing dotted disk rows with the neighbouring bare disk rows. From one modified row to the next, the positions of the polymer dots on the nanodisks were varied, from an off-center distance (i.e., distance from the center of the gold nanodisk) of about 30 nm (row 1) to about 80 nm (row 11). This implies that in rows 7, 9 and 11 the polymer dots extent over the nanodisk edge onto the substrate. Once the polymer dot starts to extend over the surface area of the disk its volume slightly increases as the height of the SU-8 layer amounts to 70 nm on the substrate and thus along the rim of the disk, while it measures only 60 nm on top of the disk. However, calculations of the resonance shift induced by 60 nm and 70 nm high polymer dots located on the top surface of the disk showed no noticeable differences (2.78 nm and 2.96 nm shift for the 60 nm and 70 nm high dots, respectively, placed at about 40 nm off-center distance), as expected due to the strong confinement of the disk near field. Thus the slightly smaller height for dots on the top surface is of minor significance when comparing the dotted rows.

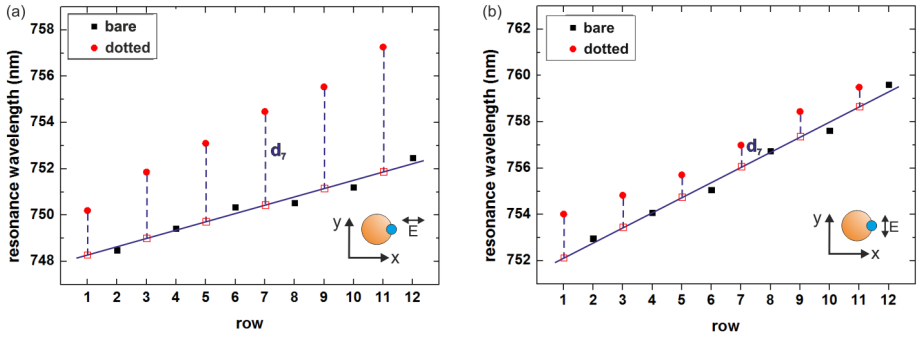


Fig. 2. Polymer dots on gold nanodisks. Resonance wavelengths of nanodisk rows for (a) x- and (b) y- polarization, as defined in the insets. The disks of every second row (full red symbols) are modified with polymer dots. The full lines are linear fits to the bare reference rows (black symbols), and the open red symbols mark the reference redshift values at the position of the dotted disks. The dashed lines show the effective spectral shift in centroid position caused by the polymer dots, with $d_7$ denoting exemplarily the shift caused by the polymer dots in row 7.

The averaged nanodisk resonance wavelengths of the sequentially measured dotted disk rows are shown in Fig. 2(a) (full red symbols). The light polarization direction is along x (for the coordinate system see inset), i.e., along the direction of the polymer dot displacement. We observe a redshift of the resonance wavelength as the polymer dots approach the disk edge, in agreement with the expected (in-plane) dipole field that increases in strength towards the disk rim. In our experiment we find a redshift as well for the bare disks (black symbols), which we could however unambiguously identify as an artifact. It is caused by a slight (and reversible) defocusing when moving from row to row due to a slightly oblique microscope table. This effect leads to a fairly linear "background" (fitted by the black line) that allows the direct extrapolation to the positions of the dotted NP rows (open red symbols) with an intercept error of the linear fit of ± 0.2 nm. We retrieve the wavelength difference between these extrapolated values and the resonance wavelengths measured for the dotted disks (full red symbol) as the redshift induced by the polymer dots. The corresponding data for the perpendicular polarization (along the y-direction) is depicted in Fig. 2(b), showing almost no spectral shifts, with even a slight decrease in redshift for the outermost dot positions. This is again in agreement with the expected dipolar plasmon field, as the strongest fields are now aligned along the y-direction, while the polymer dots are still positioned along the x-axis.

In Fig. 3 we summarize the measured effective spectral shifts of the averaged nanodisk resonances as induced by the polymer dots (full symbols). For x-polarization, the polymer dots with about 30 nm off-center distance (row 1) give rise to a resonance redshift of 2.1 nm,

#228502 - $15.00 USD Received 24 Nov 2014; revised 26 Feb 2015; accepted 3 Mar 2015; published 14 Apr 2015

whereas the dots with about 80 nm off-center distance lead to a redshift of 5.3 nm. This implies that a dot sitting halfway between disk center and rim induces only about 39% of the signal change (and thus sensitivity) due to a dot at the nanodisk rim. For y-polarization the polymer dot at about 30 nm off-center distance gives rise to a redshift of 1.9 nm, i.e., close to the corresponding x-polarization value. Moving the dot towards the disk rim leads however to decreasing redshifts, the dot with an off-center distance of about 80 nm shifts the resonance wavelength only 0.9 nm. We note that the total error of the data points was taken as ± 0.3 nm, i.e., the sum of the two error contributions discussed above.

We now corroborate our measurements with numerical simulations of a disk's local sensitivity to a dielectric dot based on the MNPBEM toolbox [20]. The backbone of this simulation package is the boundary element method [21], where an appropriate surface discretization allows solving Maxwell's equations for arbitrary particle shapes. The nanodisks (diameter 150 nm, height 30 nm) and polymer dots (diameter 50 nm, height 70 nm) were modelled according to the experimental values. The dielectric function for gold was adopted from tabulated data [22] and the refractive index of the SU-8 polymer was 1.5. The surrounding medium was assumed as homogeneous with an effective index of n = 1.2, representing a weighted average of air and the glass substrate. We increased the number of surface elements of the discretized structure until conversion was reached and refined the surface mesh particularly in the immediate vicinity of the polymer dot. When the polymer dot exceeded the boundary of the nanodisk we kept the dot at constant height and preserved its cylindrical shape (due to computational constraints), in contrast to the experimental case where the polymer dot geometry is conformally covering the disk rim and substrate. We calculated the extinction cross sections depending on the polymer dot positions and the corresponding plasmonic near fields.

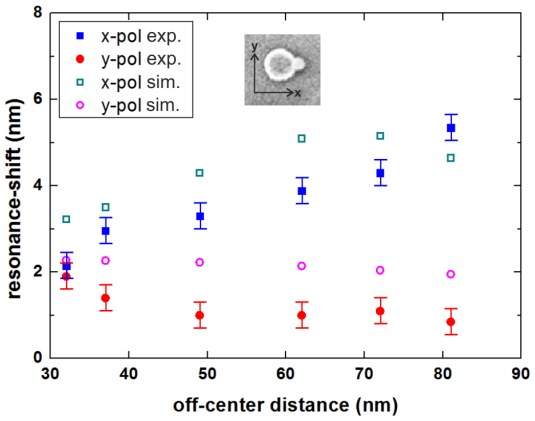


Fig. 3. Experimental and simulated shift in resonance wavelength of gold nanodisks as a function of the off-center distance of the polymer dot. The error bars comprise the uncertainty of the linear fits shown in Fig. 2 and the noise of the measurement setup. The inset shows a SEM image of a dotted nanodisk.

The simulated resonance shifts for both polarization directions are plotted in Fig. 3 as the open symbols. Both the trends and actual relative values of the experimentally observed spectral shifts are well reproduced by the simulations. The origin of the systematic larger peak shift in the simulations is likely due to the disregard of the substrate. In contrast to the case of a homogeneous medium the symmetry of the LSPR is perturbed as the electromagnetic field is stronger confined within the substrate. This leads to a reduced field acting on the polymer dot on top of the particle and thus a smaller response [23]. The simulated spectral shift for the polymer dot position around 80 nm from the disk center deviates from the trend observed for the other positions since in the simulation as the dot is kept at a constant height of 30 nm above the substrate and thus above the side of strongest field enhancement, whereas in the experimental case part of the polymer dot volume is located along the disk rim.

#228502 - $15.00 USD Received 24 Nov 2014; revised 26 Feb 2015; accepted 3 Mar 2015; published 14 Apr 2015

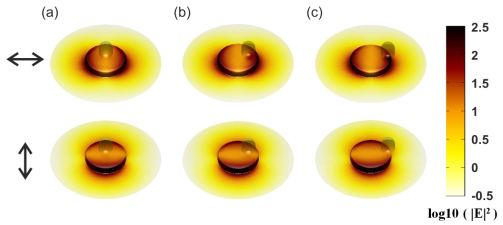


Fig. 4. Simulated plasmonic field intensities (logarithmically plotted) of dotted gold nanodisks. Shown for x-polarization (upper panels) and y-polarization (lower panels) for (a) 0 nm, (b) 37 nm and (c) 62 nm off-center distance of the polymer dot. The double arrows indicate the polarization direction.

Figure 4 shows the simulated electric near field intensity for three exemplary positions of the polymer dot on the nanodisk. The figure visualizes the plasmonic dipole field pattern and illustrates that for x-polarization the polymer dot is within the highest field intensities close to the disk rim, in contrast to the case of y-polarization. Furthermore, we find that the plasmonic field pattern is not discernibly distorted due to the presence of the polymer dot. The green dashed line in Fig. 5 shows the averaged near field intensity along the x-axis, where we vertically integrate over a window of 70 x 160 $nm^2$ (given by the dot width and height, respectively) at each dot position. The green solid curve and blue symbols show the corresponding simulated and measured resonance shifts, respectively. The simulated curve was offset by 0.9 nm towards smaller wavelengths to account for the discrepancy discussed above. Furthermore, the measured values for positive off-center distances were plotted as well for the corresponding negative position coordinates according to the mirror symmetry of the disk. One observes that the simulated data (lines) follow nicely the experimental values (symbols). In addition, an excellent match between the sensitivity curve and the profile of the electric field is observed, illustrating the strong correlation of electric field strength and local sensitivity.

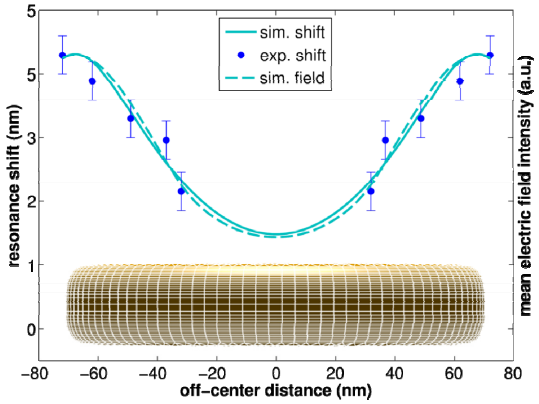


Fig. 5. Electric field and measured and simulated resonance shifts of a gold nanodisk for x-polarization. The experimental resonance shift values (symbols) were measured for positive off-center distances and plotted as well for negative coordinates due to the symmetry of the disk. The simulated spectral shift values (green line) were offset by 0.9 nm to fit to the experimental data. The profile of the electric near field intensity is shown as the dashed green line. The inset shows the disk geometry.

## 3. Masked nanodisks

Knowing the refractive index sensitivity profile of a specific NP is a basis for any kind of surface modification to control analyte access. In the case of nanodisks we aim at restricting analyte access to the disk rim where the refractive index sensitivity is highest. Therefore, we fabricated “top masked” nanodisks by covering the upper disk surface with 30 ± 1 nm high

#228502 - $15.00 USD Received 24 Nov 2014; revised 26 Feb 2015; accepted 3 Mar 2015; published 14 Apr 2015

$SiO_2$ caps (refractive index n = 1.5), leaving the disk rims free. The $SiO_2$ top caps are simply manufactured by an additional $SiO_2$ evaporation step following the deposition of gold onto the lithographed PMMA mask. Figure 6 shows schemes of the fabrication procedure and a capped nanodisk, together with a SEM image and a height profile from an atomic force microscopy measurement. To achieve uniform sensitivity along the rim we performed the following measurements with unpolarized illumination.

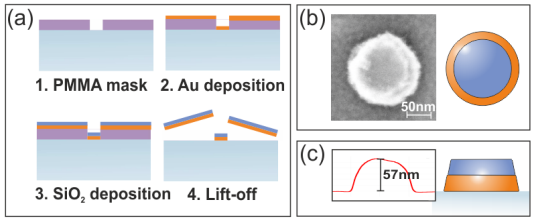


Fig. 6. Fabrication procedure of top masked nanodisks. (a) Sketch of the fabrication process. (b) SEM image and (c) height profile (by atomic force microscopy) of a nanodisk with a $SiO_2$ top mask with sketches of a masked particle.

For the sensitivity characterization of bare versus masked nanodisks, arrays of disks with diameters from 120 nm to 160 nm and a height of 30 ± 1 nm were fabricated. Optical measurements were done in transmission mode with a standard optical microscope (Zeiss, Axioskop 2) combined with a photodiode array spectrometer (MMS-1, Zeiss), and the spectral LSPR shifts were again evaluated by the centroid method. The resonance wavelengths of bare, masked and fully $SiO_2$ covered (thickness 100 nm) disks are plotted in Fig. 7(a). Looking exemplarily on the 145 ± 3 nm diameter disks we find that the 30 nm high $SiO_2$ top mask shifts the resonance by about 20 nm, whereas covering the disks completely shifts the resonance by about 64 nm. This implies that the top mask, although covering the largest part of the disk surface, induces only about 30% of the resonance shift that corresponds to the fully covered disks.

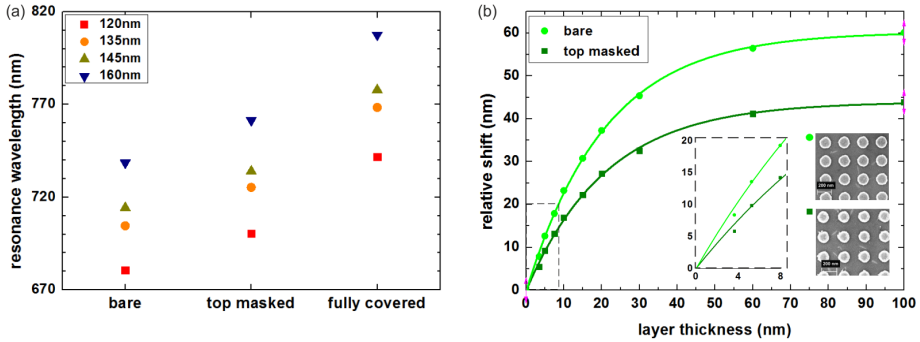


Fig. 7. Spectral shifts of masked nanodisk arrays. (a) Resonance wavelength of bare, top masked and fully $SiO_2$ covered arrays of gold nanodisks with diameters as given in the legend. (b) Shift in resonance wavelengths due to successive evaporation of thin $SiO_2$ layers on a bare and $SiO_2$ top masked array of 145 nm diameter disks. The lines are linear fits to the measured data points. The left inset in (b) shows an enlarged view of the dashed box, the right insets show SEM images of a bare (upper panel) and a $SiO_2$ top masked (lower panel) nanodisks array.

To enable a closer look on the disk sensitivity distribution, we deposited successively thin layers of $SiO_2$ on arrays of bare and top masked disks. Figure 7(b) shows the resonance wavelengths measured after each evaporation step for the 145 nm diameter disks, clearly illustrating the spectral shifts and their saturation for a layer thickness of about 60 nm [24]. The range important for molecular binding events extends only over a few nanometers closest to the disk surface. Therefore, we concentrate on the effect of the first three $SiO_2$ layers on the resonance wavelength of the top masked and bare nanodisks. The difference in spectral shifts

#228502 - $15.00 USD Received 24 Nov 2014; revised 26 Feb 2015; accepted 3 Mar 2015; published 14 Apr 2015

for the masked and bare disks amounts to 4.7 nm for a 7.5 nm thick $SiO_2$ layer, 3.4 nm for a 5 nm thick layer, and 2.3 nm for a 3.5 nm thick layer (error of all values ± 0.1 nm). These values are well approximated by a linear dependence, see the inset in Fig. 7(b). The slope of the top masked disk values amounts to about 70% of that of the bare disk values, although for a top masked disk the surface open to analyte access amounts only to 44% of the bare disk surface. This shows that covering plasmonic particles (here, the top of the disks) certainly implicates some moderate loss in overall signal, but, more importantly, leads to a gain in field uniformity (here, along the particle rim). Such a uniform and at the same time high sensitivity can be an essential condition for quantitative measurement at low concentrations, as individual molecules lead to identical spectral shifts, thus enabling the molecules to be counted. Finally, we note that since we conducted our experiments in air (n = 1), the nanodisk sensitivity to refractive index changes is higher compared with cases where the outer medium is water (n = 1.33), the basic effects are however the same.

## 4. Summary and outlook

In summary, we experimentally characterized the local refractive index sensitivity of gold nanodisks by employing a two-step lithography process to apply small polymer dots to selected positions on the disk surface. The local sensitivity distribution was mapped via the polymer-induced spectral shifts measured from particle rows. The resulting sensitivity profile shows an excellent match to the simulated electric near field intensity of the nanodisk. While it would certainly be of interest to map the sensitivity profile of plasmonic NPs with higher spatial resolution, our results so far highlight routes towards improving the sensing characteristics of plasmonic NPs, as shown with nanodisks topped with dielectric caps. Such systems with highly uniform and sensitive plasmonic modes might prove beneficial for the quantitative analysis of low analyte concentrations.

## Acknowledgments

Support by Land Steiermark (HTI MSApp, PPBioSensoren), the FWF-SFB F49 Nextlite and NAWI Graz is gratefully acknowledged.

#228502 - $15.00 USD Received 24 Nov 2014; revised 26 Feb 2015; accepted 3 Mar 2015; published 14 Apr 2015